Human influence on the increasing drought risk over Southeast Asian monsoon region

Lixia Zhang[1, 2], Ziming Chen[1,3] and Tianjun Zhou[1, 3]

1 LASG, Institute of Atmospheric Physics, Chinese Academy of Sciences, Beijing, China

2 Collaborative Innovation Center on Forecast and Evaluation of Meteorological Disasters, Nanjing University of Information Science & Technology, Nanjing, 210044, China

3 University of Chinese Academy of Sciences, Beijing 100049, China

Submitted to GRL

Revised on 8th April, 2021

Corresponding author: Lixia Zhang (lixiazhang@mail.iap.ac.cn)

Key points:

- Drought occurrence and affected area over Southeast Asian monsoon region has been increasing since 1951 in the observation.
- The human influence on the historical changes of drought risk over Southeast Asian monsoon region is detectable.
- The time of emergence of anthropogenic forcing in extreme drought occurrence and affected area occurs in the 20th century.

Abstract: Southeast Asian monsoon region is regularly stricken by drought, but less attention is paid due to its slow-onset and less visual impact. This study investigated the observed drought changes over Southeast Asian monsoon region and impacts of anthropogenic forcing using the Coupled Model Intercomparison Project phase 6 (CMIP6) models. We revealed an increasing drought risk for 1951-2018 due to more frequent and wide-spread droughts. The influence of anthropogenic forcing is successfully detected, which has increased the likelihood of the extreme droughts in historical simulation by reducing precipitation and enhancing evapotranspiration. The time of emergence of anthropogenic forcing in extreme drought occurrence and affected area occurs around the 1960s. The future projected severe and extreme drought risks are still beyond natural only forced changes under all scenarios. Our findings demonstrate a robust impact of anthropogenic forcing on drought risk over Southeast Asia, and highlight the importance of future pathway choice.

Key Words: Drought risk, Southeast Asia monsoon, CMIP6, Time of Emergence

Plain Language Summary:

As a humid region, drought in Southeast Asian monsoon region is often underestimated due to its slow rate of onset and less visual impact. Here we revealed a significant increasing trend of drought occurrence and affected area over Southeast Asian monsoon region since the 1950s. The impact of human influence is successfully detected using the Coupled Model Intercomparison Project phase 6 (CMIP6) models. Anthropogenic forcing has increased the likelihood of the extreme droughts for 1951-2014 by suppressing water supply and enhancing evaporation demand. The time of emergence of anthropogenic forcing in extreme drought frequency and affected area firstly appeared around the 1960s. Even though drought risk will start to decrease since the 2030s in the future under the lowest emission scenario of CMIP6, the projected drought risks are still beyond natural only forced changes.

1. Introduction

Southeast Asian monsoon region falls in the warm and humid tropics modulated by Asian monsoon. It is home to nearly 15% of the world's tropical forests and 8.5% population in 3% earth's total land area, and also one of the biodiversity hotspots in the world (Stibig et al., 2014; Sodhi et al., 2010). With the unprecedented urbanization and population growing rate, water scarcity issues have already posed a serious challenge for sustainable development in Southeast Asian monsoon region (Kumar et al., 2015). As a humid region, drought in this region is often underestimated due to its slow rate of onset and less visual impact. However, drought can have devastating cumulative impacts, especially on the countries which are poor and less developed but heavily depend on agriculture (Polpanich, 2010). Thus, understanding the drought changes and the behind mechanism are of great importance.

This study focuses on the Southeast Asian monsoon region, including the mainland Southeast Asian countries and South China (10~30°N, 90~120°E) (Fig.1a-b), because this region has the longest wet season and the strongest interannual variability in the monsoon length in the Asian monsoon region (Misra and DiNapoli 2013). Decreasing trends in annual precipitation from the 1950s to 2000s were observed in Myanmar, Thailand and northern Vietnam (Endo et al., 2009), and the number of rainy days was significantly decreased over Southeast Asia from 1961 to 1998 (Manton et al., 2001). Drought has affected over 66 million people in Southeast Asian countries for the past 30 decades (ASEAN, 2019). The 2020 drought started from 2019 has caused water levels in Southeast Asia's Mekong River

to drop to its lowest in more than 100 years (https://www.nationalgeographic.com/environment/2019/07/mekong-river-lowest-levels-100-years-food-shortages/), affecting 13 provinces in the Mekong Delta region (https://reliefweb.int/report/viet-nam/viet-nam-drought-and-saltwater-intrusion-office-resident-coordinator-flash-update-1). The 2020 drought also spread to Southwest China, the upstream of Mekong River, and over one million people were lack of accessing drinking water (https://news.cgtn.com/news/2020-04-05/Drought-affects-over-one-million-people-in-SW-China-province-PrpBkhlJok/index.html). South China, adjacent to the Southeast Asian countries, has been frequently stricken by droughts in recent decades (Xin et al., 2008; Zhang et al., 2013; Chen and Sun, 2015; Zhang et al., 2020). The two adjacent regions share the same climate and are facing similar drought risk. Thus, we study the drought changes over the traditional Southeast Asian countries and South China together in this study.

Climate change could further aggravate drought by either enhancing evapotranspiration or suppressing precipitation (Dai, 2011; Trenberth et al., 2014), and Southeast Asian monsoon region is one of the hotspots with strong drying under global warming (Cook et al., 2020). The effect of black carbon aerosol radiative forcing can partly explain the observed drying trend of Southeast Asian spring precipitation (Lee and Kim, 2010). The optimal fingerprinting attribution shows a dominant role of anthropogenic aerosols forcing in the declining trend since the 1950s of northern hemispheric monsoon precipitation, including Southeast Asia (Polson et al., 2014). Compared with present-day, drought events are projected to increase in the future over mainland Southeast Asia based on the regional

88 climate model (Amnuaylojaroen and Chanvichit, 2019) and CMIP5 multimodel simulations
89 (Lu et al., 2019). As for the droughts associated with El Niño events, drought would cover
90 more area over Southeast Asia in thenear future even with less severe El Niño events, and
91 droughts associated with severe El Niño would be more extreme and more widely spread in
92 the near and far future (Hariadi, 2017).

93 The Coupled Model Intercomparison Project phase 6 (CMIP6) with improved climate
94 models and more modelling groups is expected to provide more reliable information on the
95 regional climate response to anthropogenic forcing (Eyring et al., 2016; Ukkola et al.,
96 2020). This study aims to answer the following questions by examining observation and
97 CMIP6 multimodel output: 1) How does the observed drought over Southeast Asian
98 monsoon region change since the 1950s? 2)Whether anthropogenic forcing plays any role in
99 the drought changes? 3) How would drought change under different scenarios in the future?

100 **2. Data and Method**

101 ***2.1 Observation and CMIP6 model simulations***

102 We use monthly observational precipitation and potential evapotranspiration dataset from
103 the Climatic Research Unit of the University of East Anglia (CRU TS v.4.03) for 1951-2018
104 at a horizontal resolution of 0.5º (Harris et al., 2020). To verify the observed drought
105 changes revealed by SPEI, the surface (0-10cm) soil moisture from Global Land Data
106 Assimilation System Version 2 (GLDAS-2.0, Rodell et al. 2004; Beaudoing et al. 2019) for
107 1951-2014 is also used. We employ the pre-industrial control simulation (piControl),

historical simulation (Hist) and four future scenarios projections from 14 coupled models underpin CMIP6 to explore the role of anthropogenic forcing and the scenario dependence of drought changes in future projection (Table S1-2). The four scenarios chosen in this study are the Shared Socioeconomic Pathways (SSP) 1-2.6, 2-4.5, 3-7.0 and 5-8.5 (O'Neill et al., 2016). The piControl is employed to estimate internal variability of the unforced drought. All model outputs are interpolated onto the same resolution of 1.5°×1.5° using the first-order conservative interpolation. We use Hargreaves equation to calculate reference evapotranspiration (ET) (Hargreaves, 1994), which has a good agreement with Penman-Monteith method (Droogers and Allen, 2002).

This study chooses the Standardized Precipitation-Evapotranspiration Index (SPEI, Vicente-Serrano et al., 2010a, b) to investigate the changes in drought intensity, occurrence or frequency defined as drought months per year and affected area fraction. To verify the observed drought changes revealed by SPEI, self-calibrating Palmer Drought Severity Index (sc-PDSI, Wells et al., 2004) is also employed. In observation, SPEI and sc-PDSI are both calculated based on the CRU TSv.4.03 precipitation and evapotranspiration dataset (Vicente-Serrano et al., 2010b; Schrier et al., 2013). As monthly sc-PDSI is not able to depict drought on time scales shorter than 12 months, we use SPEI at a 12-month time scale to estimate drought changes in the observation. In each model simulation, SPEI is calculated using a Log-Logistic distribution (Vicente-Serrano et al., 2010a), the parameters of which are derived by fitting it to the piControl simulations of that model.

2.2 Estimate of internal variability and Time of Emergence

129 Following Zhang and Delworth (2018), internal variability is estimated from multi-
130 millennia preindustrial control simulations. For drought occurrence and affected area
131 changes, we first calculate the drought occurrence at each grid and the drought affected area
132 of the study area. The running-mean drought affected area and area-averaged drought
133 frequency for a 20-yr period over the target region are then calculated. Internal variability is
134 defined as the range between the maximum and minimum values across the entire piControl
135 runs, respectively. The results are only caused by internal climate variability. For internal
136 variability of the changes in precipitation, we first randomly select two non-overlapping 20-
137 yr periods from the piControl simulation. Then, we calculate the difference between these
138 two 20-yr periods. Next, we repeat these 14 times (to mimic the 14 models ensemble) to
139 form the ensemble and compute ensemble average. Finally, we repeat the above process
140 5000 times to gain a probability density function (PDF) of internal variability.

141 The time of emergence (TOE) is defined as the time when external forcing signal, which is
142 represented by multimodel ensemble mean (MME), exceeds internal variability firstly and
143 lasts at least 2 decades (Zhang and Delworth 2018). To estimate the spread of TOE, we
144 calculate the time when the MME exceeds ranges of internal variability of each model, and
145 define this time as the TOE for each model. The spread of TOE is the range of ±1 standard
146 deviation of TOE across the 14 models.

147 **3. Results**

148 **3.1 Observed drought changes for 1951-2018**

149 In observation, an overall drying trend over the Southeast Asian monsoon region is observed
150 since the 1950s, with the strongest drying trend over Yunnan Province in China, northern
151 Thailand and Myanmar (Fig.1a). SPEI has decreased by -0.75 at the maximum from 1951 to
152 2018. The occurrence of extreme drought, defined as month with SPEI≤-2.0 per year, has
153 been significantly increasing over the regions with significant decreasing trend of SPEI
154 (Fig.1b). It is centered over the Southwest China and Burma. In contrast, Viet Nam, along
155 the east coast of Pacific Ocean, show significant wetting trends. Significant increasing
156 trends in the drought occurrence and affected area are seen from the temporal changes
157 averaged over Southeast Asia (Fig.1c-d). For the past 68 years, the severe and extreme
158 drought occurrence (affected area) has increased by 0.8 and 0.2 month per year (7.1% and
159 3.1%), respectively, approximately 23% and 8% (85% and 142%) of climate mean. In
160 contrast, the linear trend in drought intensity is insignificant (Fig.S1a). So, we will mainly
161 focus on the changes in drought occurrence and affected area in the following sections.

162 The results based on sc-PDSI (Fig.S1b and Fig.S2) and surface soil moisture (Fig.S3) both
163 confirm the increasing drought risk over Southeast Asian monsoon region. Following Cook
164 et al. (2014), we recalculate SPEI by removing the linear trend of ET for 1901-2018 to
165 estimate contribution of precipitation changes to the drought risk trend (Fig.S4). Over the
166 centers with strongest decreasing trend of SPEI and increasing trend of drought occurrence,
167 the contribution of precipitation changes is higher than 50%, reaching 0.9 at maximum,
168 demonstrating the importance of precipitation changes. Given the high consistency between
169 sc-PDSI and SPEI, we will use SPEI to investigate the impact of anthropogenic forcing in

170 the following discussion.

171 **3.2 Responses of droughts to historical anthropogenic forcing**

172 By comparing PDF distributions of drought indices averaged over the study region in Hist
173 and piControl, a detectable role of anthropogenic forcing can be seen from the leftward
174 (rightward) shift in SPEI, precipitation and surface soil moisture (ET, drought occurrence
175 and affected area) under anthropogenic forcing (Fig.2a-b). The likelihood of a 1-in-20-yr
176 drought event defined by extreme drought occurrence and affected area in piControl is
177 estimated to increase to 24% (6%~49% for 10th-90th confidence level) and 32% (25% to
178 45%) in Hist, respectively. It indicates anthropogenic forcing has increased the risk of such
179 event by 5-time (3~25-time) and 6-time (4~9-time) estimated from risk ratio ($P_{Hist}/P_{piControl}$),
180 respectively. Human influence can intensify the drought risk by increasing both standard
181 deviation and climate mean of precipitation, ET and SPEI (horizontal lines Fig.2a-c).
182 Specifically, standard deviation for SPEI, precipitation anomaly and ET anomaly in Hist
183 increases to 0.44, 0.81 mm day^{-1}, and 0.15 mm day^{-1} from 0.40, 0.77 mm day^{-1}, and 0.13 mm
184 day^{-1} in piControl.

185 **3.3 ToE of anthropogenic forcing**

186 To investigate when the human influence forced signal exceeds natural variability, we
187 estimate the TOE of anthropogenic forcing here. Because estimation of TOE is sensitive to
188 the simulated ranges of climate variability, we firstly evaluate the models' capability in
189 simulating the variability of drought occurrence and affected area over Southeast Asian

190 monsoon region. Most CMIP6 models and MME underestimate the variability of
191 occurrence of extreme drought, but overestimate the extreme and severe drought affected
192 area fraction (Fig.S5). To avoid the model biases, we scale the simulated variability of
193 internal variability using the ratio between the standard deviation of observation and of Hist
194 of each model for the period 1950-2018.

195 Consistent with the observation, a significant increasing trend for the drought occurrence
196 and affected area fraction since the early 20th century is clearly simulated in Hist. The TOE
197 of climate change induced extreme drought occurrence and affected area emerges around
198 1967 (1928~2006) and 1967 (1941~1993), close to that of severe drought events 1969
199 (1935~2003) and 1967 (1939~1995). We also investigate whether future changes in drought
200 risk under different scenarios will return to natural only forced variability (colored lines in
201 Fig.3). The extreme and severe drought occurrence and area fraction start to decrease
202 around the 2030s under SSP1-2.6 and keep stable since the 2030s under SSP2-4.5, while
203 continue to increase through the whole 21st century under SSP3-7.0 and SSP5-8.5. The
204 anthropogenic forced higher drought risks are still beyond the ranges of natural variability
205 of piControl under the four scenarios, although a decrease is shown in SSP1-2.6. The largest
206 increase is seen from SSP3-7.0, which has the greatest anthropogenic aerosol loadings in the
207 future (Wilcox et al. 2020). The drought will become more frequent and more widespread in
208 the future compared with piControl under all scenarios, but a slight decrease relative to
209 present day is projected under the lowest emission scenarios. The earliest TOE has appeared
210 over the Southwest China before the 1990s, followed by the Mekong river basin countries

211 (Fig.S6a). For the drought occurrence changes averaged over the 20 years around TOE
212 relative to piControl, extreme drought increases by 0.4 ~ 0.8month per year over the
213 Southwest China and 0.4~1 month over Thailand (Fig.S6b).

214 We also present the changes of precipitation, ET and their difference (PmE) relative to
215 piControl to see their impact on drought risk changes(Fig.4). In the 20th century, the
216 ensemble mean precipitation of the 14 CMIP6 models shows very similar evolution to those
217 in drought, decreasing with time from the early 21st century to present, reaching its
218 minimum recently. The TOE of precipitation occurs around 1980 (1973~1987) (Fig.4a).
219 Meanwhile, the anthropogenic activity forced ET increases with time and goes beyond
220 natural variability around 1999 (1968~2030), with much weaker magnitude than
221 precipitation (Fig.4b). The combination of decrease in water supply (precipitation) and
222 increase in evaporation demand (ET) contributes to the decreasing trend in PmE (Fig.4c).

223 As for the future projection, precipitation shows a recovery since the 2020s in all scenarios
224 except SSP3-7.0 under which it recovers from the 2030s. Changes in precipitation return to
225 the ranges of natural variability around 2030 (2025~2035), 2037 (2031~2043), 2059
226 (2054~2064), 2039 (2032~2046) in SSP1-2.6, SSP2-4.5, SSP3-7.0, and SSP5-8.5,
227 respectively (colored lines in Fig.4a), and even exceeds internal variability around 2080 in
228 SSP5-8.5. In comparison, ET in all scenarios keeps on increasing with a faster rate under
229 stronger anthropogenic forcing (Fig.4b). The changes in PmE under SSP2-4.5 and SSP3-7.0
230 do not return to the ranges of internal variability because of faster ET increase and
231 moderated recovery of precipitation with global warming (Table S3). The changes in

232 precipitation, ET and PmE demonstrate that future global warming benefits a recovery of
233 Southeast Asian monsoon precipitation, but faster ET increase could overwhelm its recovery
234 and contribute to a further decrease in PmE and higher drought risk.

235 Similar to drought changes, the earliest TOE of decreased precipitation is also seen over
236 Southwest China (Fig.S7a-b). Under SSP1-2.6, SSP2-4.5 and SSP5-8.5, eastern part of
237 South China and Mekong River would return to the ranges of natural variability around
238 2040 (Fig.S7c-f). Under SSP3-7.0, the area with precipitation returning to internal
239 variability is the smallest (Fig.S7e).

240 Enhancement of precipitation in the future projection is closely related to radiative forcing.
241 In Hist, reduction in precipitation is dominated by anthropogenic aerosol forcing by
242 reducing atmospheric humidity and weakening the monsoon circulation, although the
243 thermodynamic effect from greenhouse gases forcing can partly offset the impact of
244 anthropogenic aerosol forcing (Zhou et al., 2020). In the future projection, greenhouse gases
245 (GHGs) keep on increase but anthropogenic aerosol forcing declines (O'Neill et al., 2016),
246 which intensifies the impact of GHGs on precipitation through the thermodynamic response
247 (Chen et al., 2020; Wilcox et al., 2020), and enhances ET as well. Higher scenarios result in
248 faster warming, and faster recovery in precipitation and enhancement in ET. Only under
249 SSP1-2.6 and SSP5-8.5, the recovery of precipitation exceeds enhanced ET, favorable of
250 less drought risk and a return to the variability in a natural world.

251 **4. Summary and conclusion remarks**

252 As a slow-onset extreme event, drought over Southeast Asian monsoon region is paid less
253 attention so far. We examined drought changes over this region in the observation from 1950
254 to 2018, and showed that Southeast Asian monsoon region has been undergoing more
255 frequent and more wide-spread drought for 1951-2018 in the observation, centered
256 Southwest China, northern Thailand and Myanmar. The extreme drought affected area
257 fraction are almost doubled during 1951-2018 over the study region.

258 The impact of anthropogenic forcing and projected changes in drought under different
259 scenarios were investigated by comparing Hist and future projections with piControl from
260 the CMIP6 multimodel output. We found a detectable role of anthropogenic forcing on the
261 increasing drought risk over the Southeast Asian monsoon region. Human influence has
262 increased the occurrence and affected area fraction of extreme drought during 1951-2014.
263 Consistent with the observation, significant increasing trends for the drought occurrence and
264 affected area fraction in Hist are simulated since the early 20th century. The TOE of extreme
265 drought occurrence and affected area appeared around 1967 (1928~2006) and 1967
266 (1941~1993), respectively. The anthropogenic forced precipitation decrease dominates the
267 increasing drought risk in the past century. In the future, the projected changes in extreme
268 and severe drought risk would start to decrease around the 2030s under SSP1-2.6, while
269 keep on increasing through the whole 21st century under SSP3-7.0 and SSP5-8.5. However,
270 the projected changes in drought risk under all scenarios are still beyond the ranges of
271 natural variability.

272 Our study demonstrated a distinguishable role of anthropogenic forcing in the increasing

273 drought risk over Southeast Asian monsoon region, and the TOE of anthropogenic forcing
274 on drought has occurred in the past. Both higher aerosols loading and higher radiative
275 forcing in the future are important for the drought changes, and SSP3-7.0, which bears the
276 largest anthropogenic aerosol loadings in the future and second high radiative forcing
277 among the four scenarios, projects the most frequent and most widespread drought for the
278 mid- and long-term projections. Although precipitation over Southeast Asian monsoon
279 region will recover since the 2050s due to more atmospheric humidity with global warming,
280 the evapotranspiration enhancement could offset and even overwhelm the precipitation
281 recovery, increasing the drought risk.

282 Southeast Asian monsoon region, particular over the Mekong river Basin, will be the
283 hotspot of frequent and widespread drought risk in the future. It would greatly threaten the
284 agriculture, heightened fire risks and lead to acute shortages of drinking water. ASEAN and
285 the United Nations Economic and Social Commission for Asia and the Pacific proposed to
286 build resilience to drought in Southeast Asia mitigate the impacts of drought (UN, 2020).
287 Here, we demonstrate the choice of pathways is also crucial for the drought risk changes
288 over Southeast in the future. It is urgent to take actions to reduce anthropogenic aerosol
289 loading and greenhouses gases emissions to reduce the Southeast Asian drought risks.

290 **Acknowledgement:**

291 This work was jointly supported by the Ministry of Science and Technology of China under
292 Grant 2018YFA0606501 and National Natural Science Foundation of China under grant No.
293 42075037. We acknowledge the World Climate Research Programme's Working Group on

294 Coupled Modeling, which is responsible for CMIP6, and the climate modeling groups
295 (listed in Table S1) for producing and making available their model output (https://esgf-
296 node.llnl.gov/search/cmip6/). We also thank University of East Anglia Climatic Research
297 Unit (CRU) for providing the observational precipitation datasets
298 (https://catalogue.ceda.ac.uk/uuid/10d3e3640f004c578403419aac167d82). The SPEI and sc-
299 PDSI datasets can be freely accessed from the websites
300 (https://spei.csic.es/spei_database.html and https://crudata.uea.ac.uk/cru/data/drought/).
301 Surface soil moisture from GLDAS is available from
302 https://disc.gsfc.nasa.gov/datasets/GLDAS_NOAH025_M_2.1/summary.

303 **References:**

304 Amnuaylojaroen Teerachai and Pavinee Chanvichit (2019) Projection of near-future climate
305 change and agricultural drought in Mainland Southeast Asia under RCP8.5. Climatic
306 Change, 155:175-193.

307 Beaudoing, H. and M. Rodell, NASA/GSFC/HSL (2019), GLDAS Noah Land Surface
308 Model L4 monthly 0.25 x 0.25 degree V2.0, Greenbelt, Maryland, USA, Goddard
309 Earth Sciences Data and Information Services Center (GES DISC), Accessed:
310 [https://disc.gsfc.nasa.gov/datasets/GLDAS_NOAH025_M_2.1/summary, last accessed
311 on 25th January 2021], 10.5067/9SQ1B3ZXP2C5

312 Chen H, and J Sun (2015) Changes in Drought Characteristics over China Using the
313 Standardized Precipitation Evapotranspiration Index. J. Climate, 28, 5430–5447.

314 Chen Z. M., T. J. Zhou, L. X. Zhang, et al. (2020) Global land monsoon precipitation
315 changes in CMIP6. Geophysical Research Letters, 47, e2019GL086902. https://doi.org/
316 10.1029/2019GL086902

317 Cook B. I., J.E. Smerdon, R. Seager., et al. 2014: Global warming and 21st century drying.
318 Clim. Dyn. 43: 2607-2627.

319 Cook B. I., Mankin, J. S., Marvel, K., Williams, A. P., Smerdon, J. E., & Anchukaitis, K. J.
320 (2020) Twenty-first century drought projections in the CMIP6 forcing scenarios.
321 Earth's Future. 8, e2019EF001461. https://doi.org/10.1029/2019EF001461

322 Dai A. (2011) Drought under global warming: A review Wiley Interdiscip. Rev. Clim.
323 Chang. 2 45–65.

324 Droogers P. and R. Allen (2002) Estimating reference evapotranspiration under inaccurate
325 data conditions. Irrigation and Drainage Systems 16: 33–45.

326 Eyring, V., Bony, S., Meehl, G. A., Senior, C. A., Stevens, B., Stouffer, R. J., and Taylor, K.
327 E. (2016) Overview of the Coupled Model Intercomparison Project Phase 6 (CMIP6)
328 experimental design and organization, Geosci. Model Dev., 9, 1937–1958,
329 https://doi.org/10.5194/gmd-9-1937-2016.

330 Hariadi M. H. (2017) Projected drought severity changes in Southeast Asia under medium
331 and extreme climate change. Wageningen University and Research, and Royal
332 Netherlands Meteorological Institute, Ministry of Infrastructure and the Environment,
333 KNMI Scientific Report WR-2017-02. (M.Sc. thesis report). Available from:

334 http://bibliotheek.knmi.nl/knmipubWR/WR2017-02.pdf.

335 Harris I., T. J. Osborn, P. Jones, and D. Lister (2020) Version 4 of the CRU TS monthly
336 high-resolution gridded multivariate climate dataset. Scientific Data, 7, 109(2020).
337 https://doi.org/10.1038/s41597-020-0453-3

338 Juneng, L. and Tangang, F. (2005) Evolution of ENSO-related rainfall anomalies in
339 Southeast Asia region and its relationship with atmosphere–ocean variations in Indo-
340 Pacific sector, Clim. Dyn., 25, 337–350.

341 Kumar M. D., P. K. Viswaathan and Nitin Bassi (2015) Water Scarcity and Pollution in
342 South and Southeast Asia: Problems and Challenges, in Paul G. Harris and Graeme
343 Lang (eds.), Routledge Handbook of Environment and Society in Asia, Routledge,
344 Taylor & Francis Group, London, pp. 197-215.

345 O'Neill, B. C., Tebaldi, C., van Vuuren, D.P., Eyring, V., Friedlingstein, P., Hurtt, G., Knutti,
346 R., Kriegler, E., Lamarque, J.-F., Lowe, J., Meehl, G.A., Moss, R., Riahi, K., and
347 Sanderson, B. M. (2016) The Scenario Model Intercomparison Project (ScenarioMIP)
348 for CMIP6. Geosci. Model Dev., 9: 3461-3482.

349 Räsänen, T. A. and Kummu, M.(2013) Spatiotemporal influences of ENSO on precipitation
350 and flood pulse in the Mekong River Basin, J. Hydrol., 476, 154–168.

351 Rodell, M., P.R. Houser, U. Jambor, J. Gottschalck, K. Mitchell, C. Meng, K. Arsenault, B.
352 Cosgrove, J. Radakovich, M. Bosilovich, J.K. Entin, J.P. Walker, D. Lohmann, and D.
353 Toll, 2004: The Global Land Data Assimilation System, Bull. Amer. Meteor. Soc., 85,

354 381-394, doi:10.1175/BAMS-85-3-381

355 Schrier G. van der, J. Barichivich, K. R. Briffa, P. D. Jones (2013) A scPDSI-based global
356 data set of dry and wet spells for 1901-2009. J. Geophys. Res. Atmos., 118, 4025–
357 4048, doi:10.1002/jgrd.50355.

358 Sodhi, N. S. et al. (2010) The state and conservation of Southeast Asian biodiversity.
359 Biodivers. Conserv. 19, 317–328.

360 Stibig, H. J., Achard, F., Carboni, S., Rasi, R. & Miettinen, J. (2014) Change in tropical
361 forest cover of Southeast Asia from 1990 to 2010. Biogeosciences 11, 247–258.

362 Trenberth, K. E., A. Dai, G. van der Schrier, P. D. Jones, J. Barichivich, K. R. Briffa, and J.
363 Sheffield (2014) Global warming and changes in drought. Nature Climate Change, 4,
364 17-22

365 Ukkola A. M., M. G. D. Kauwe, M. L. Roderick, G. Abramowitz, A. J. Pitman (2020)
366 Robust Future Changes in Meteorological Drought in CMIP6 Projections Despite
367 Uncertainty in Precipitation. Geophysical Research Letters, 47, e2020GL087820,
368 https://doi.org/10.1029/2020GL087820.

369 Vicente-Serrano S.M., Beguería S., López-Moreno J.I., (2010a) A Multi-scalar drought
370 index sensitive to global warming: The Standardized Precipitation Evapotranspiration
371 Index-SPEI. Journal of Climate, 23(7), 1696-1718, DOI: 10.1175/2009JCLI2909.1.
372 http://digital.csic.es/handle/10261/22405.

373 Vicente-Serrano S.M., Beguería S., López-Moreno J.I., Angulo M., El Kenawy A. (2010b) A

374 global 0.5° gridded dataset (1901-2006) of a multiscalar drought index considering the
375 joint effects of precipitation and temperature. Journal of Hydrometeorology 11(4),
376 1033-1043, DOI: 10.1175/2010JHM1224.1. http://digital.csic.es/handle/10261/23906.

377 Wang B., M. Biasutti, M. P. Byrne, et al. (2020) Monsoon Climate Change Assessment.
378 Bull. Amer. Meteor. Soc., https://doi.org/10.1175/BAMS-D-19-0335.1.

379 Wang Lin, Chen Wen, Zhou Wen, Huang Gang (2015) Understanding and detecting super
380 extreme droughts in Southwest China through an integrated approach and index. Q. J.
381 R. Meteorol. Soc., 142: 529–535, DOI: 10.1002/qj.2593.

382 Wells N., Goddard S. and Hayes M.J. (2004) A self-calibrating Palmer Drought Severity
383 Index. Journal of Climate, 17, 2335-2351

384 Xin X., R. Yu, T. Zhou, and B. Wang (2006) Drought in late spring of South China in recent
385 decades. J. Climate, 19, 3197–3206, https://doi.org/10.1175/JCLI3794.1.

386 Zhang H., & Delworth, T. L. (2018). Robustness of anthropogenically forced decadal
387 precipitation changes projected for the 21st century. *Nat Commun, 9*(1), 1150.
388 https://doi.org/10.1038/

389 Zhang L., Zhou T., Chen X., Wu P., Christidis N., Lott F. (2020). The late spring drought of
390 2018 in South China, Bull. Amer. Met. Soc., 101(1): S59-S64. DOI:10.1175/BAMS-D-
391 19-0202.1.

392

393

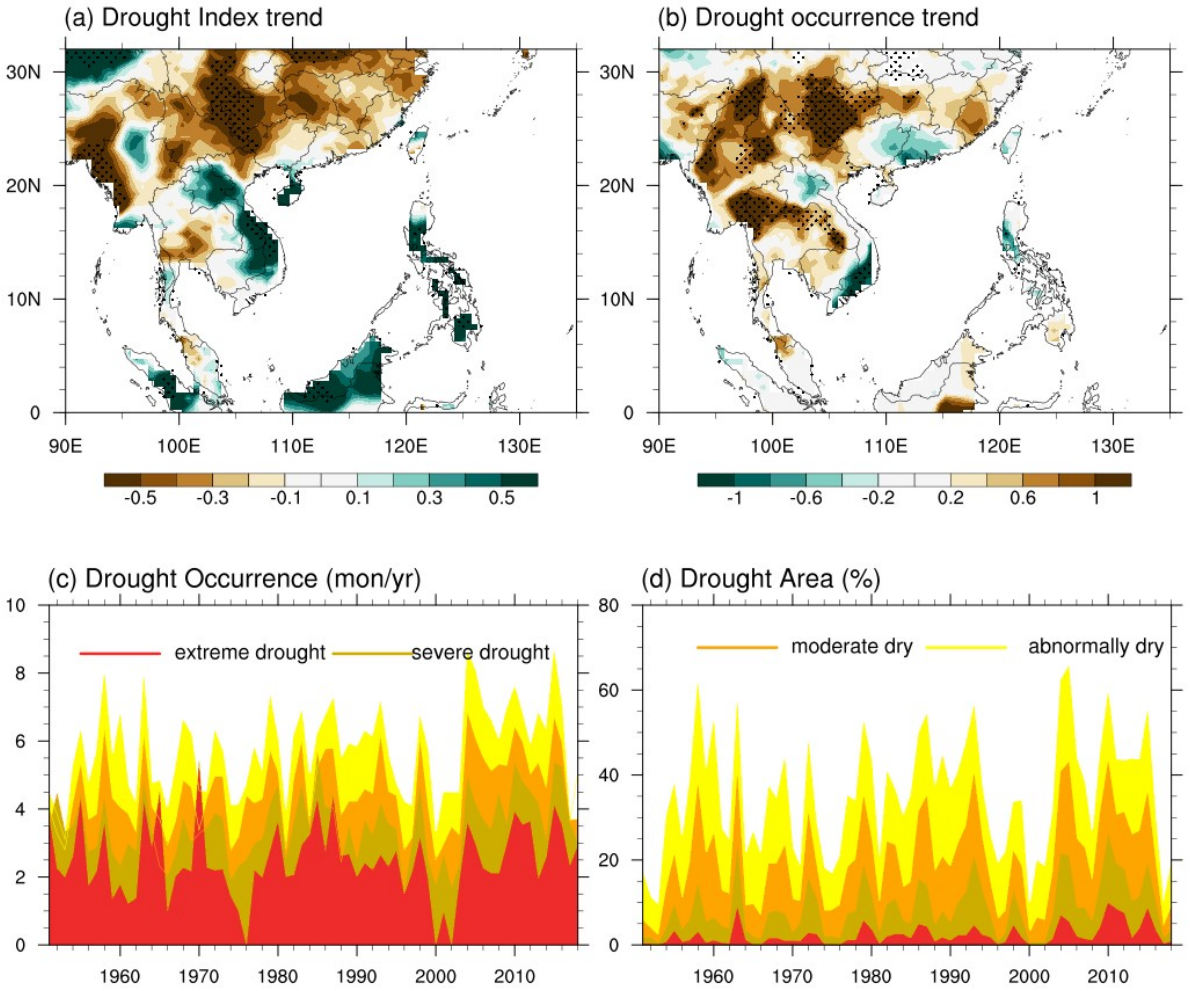

394

395

396 **Fig. 1** The spatial distribution for observed linear trend of drought from 1951 to 2018 for (a)
397 SPEI (unit: $(68yr)^{-1}$) (b) extreme drought (SPEI≤-2.0) occurrence (unit: month $(68yr)^{-1}$). (c)-
398 (d) are the temporal changes of (c) occurrence (unit: month yr^{-1}) and (d) affected area
399 fraction (unit: %) for different drought categories averaged over Southeast Asian monsoon
400 region (10-30°N, 90-120°E). The yellow, orange, brown and red lines represent abnormally
401 dry (SPEI≤-0.5), moderate drought (SPEI≤-1.0), severe drought (SPEI≤-1.5), and extreme
402 drought (SPEI≤-2.0), respectively.

403

404

405

406

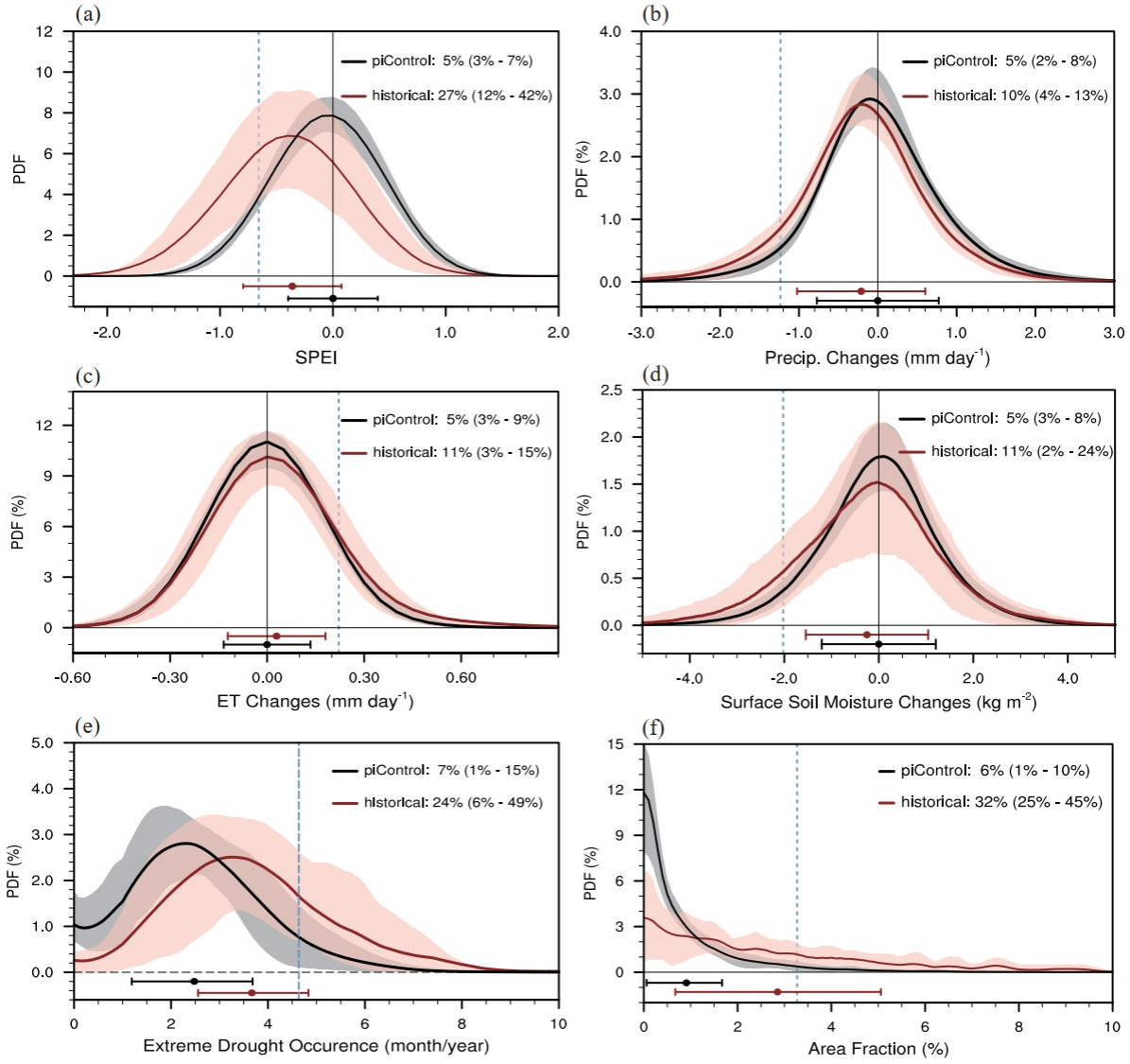

Fig.2 Probability distribution function (PDF) of drought changes in piControl and Hist. (a) SPEI averaged over the land area of Southeast Asian monsoon region. (b)-(c) are same as (a), but for annual mean precipitation (mm day^{-1}), ET (mm day^{-1}) and surface soil moisture (0-10cm) (kg m^{-2}) anomalies relative to piControl. (e)-(f) are for extreme drought occurrence and affected area fraction over the Southeast Asian land monsoon region. The solid lines are the multi-model ensemble (MME) mean of piControl (black line) and Hist for 1950-2014 (red line), and the shadings denote the range of 10th to 90th across models. The vertical blue dash lines denote the return value of 20-yr period. The horizontal lines and dots denote the range of standard deviation and the mean value of PDFs, respectively. The mean value and the inter-model 10th-90th range are shown in the right corner of each plot.

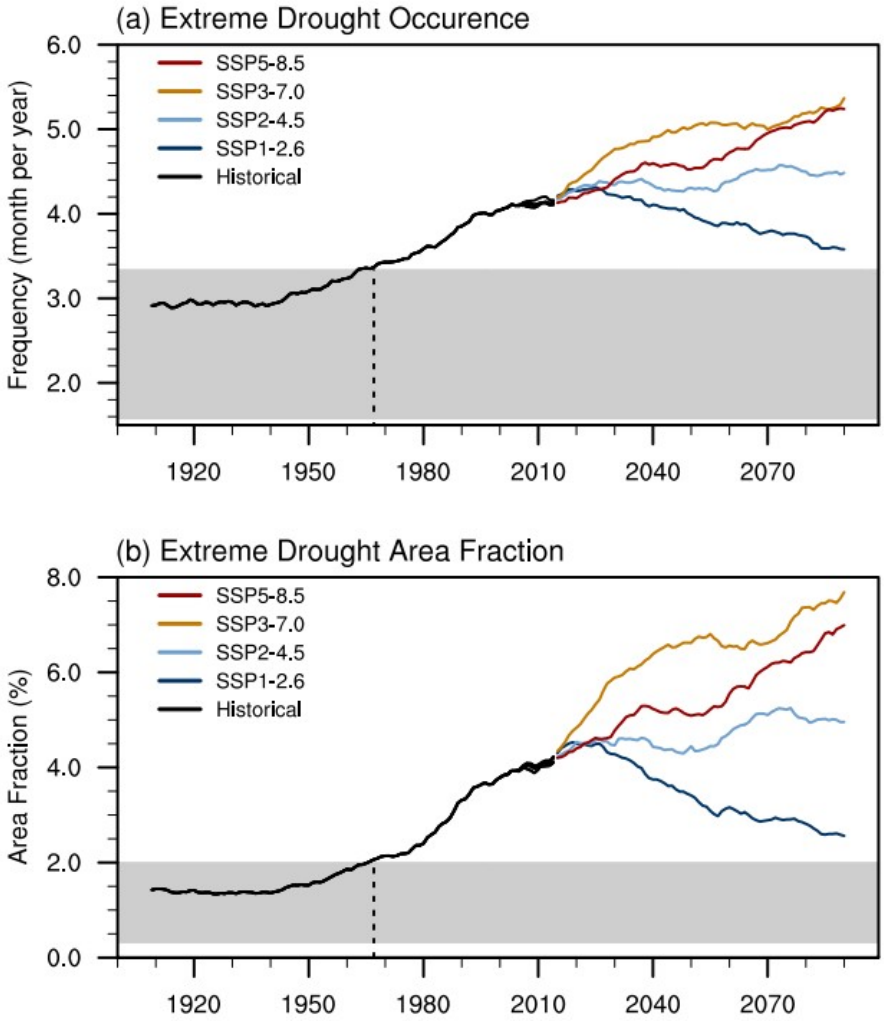

Fig.3 The 20-yr running mean changes in extreme drought (a) occurrence (month year^{-1}) and (b) affected area fraction (%) over the Southeast Asian monsoon region in Hist (black) and four future projections (colored lines) based on multi-model ensemble (MME) of the 14 CMIP6 models. The gray shadings denote the range of internal variability, which has been corrected by the ratio between the standard deviation of observation and Hist in 1950~2014 (FigS5). The dark blue, light blue, brown and red are for SSP1-2.6, SSP2-4.5, SSP3-7.0 and SSP5-8.5, respectively. The black vertical dash lines denote the time of emergence (TOE).

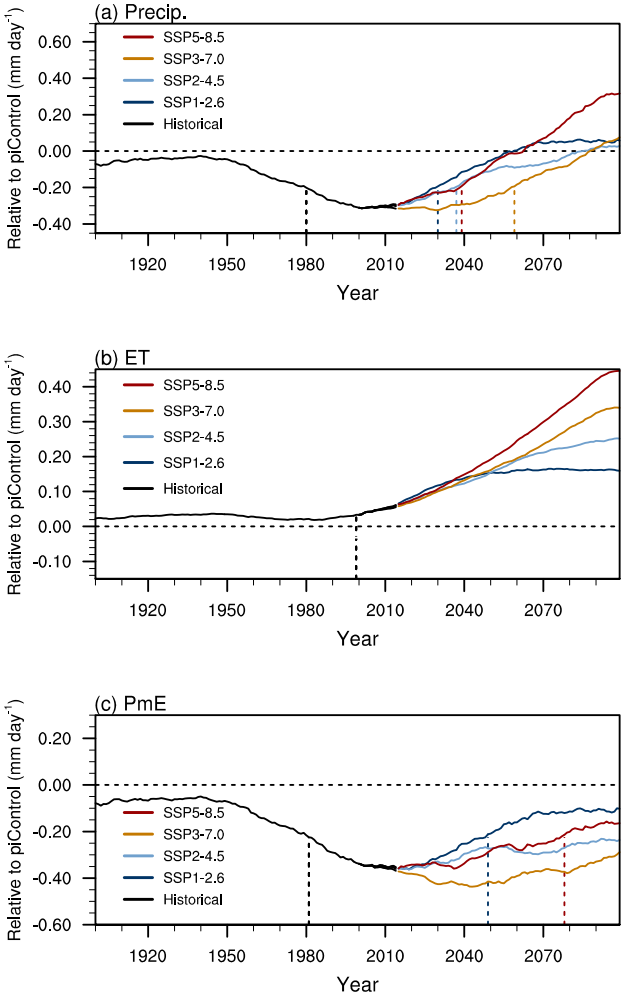

429

430 **Fig. 4** Same as Fig.3, but for the changes in anomalous annual mean (a) precipitation (P),
431 (b) evapotranspiration (ET) and (c) P minus ET (PmE) area-averaged over the Southeast
432 Asian monsoon region relative to piControl.

433